

# 3D-Printed prosthesis for recurrent femoral metastasis with periprosthetic infection: A case report

JIANGBI LI<sup>1</sup>, YANGJIE ZHANG<sup>1</sup>, JIANPING KANG<sup>1</sup>, CHANGPING TIAN<sup>1</sup>,  
SUOLIN CHEN<sup>1</sup>, YA NING<sup>1</sup>, HAIXIA LI<sup>2</sup> and YANBIN XIAO<sup>1</sup>

<sup>1</sup>Department of Orthopaedics, Yunnan Cancer Hospital, The Third Affiliated Hospital of Kunming Medical University, Kunming, Yunnan 650118, P.R. China; <sup>2</sup>Department of Neurology, The First People's Hospital of Yunnan Province, Kunming, Yunnan 650118, P.R. China

Received September 14, 2025; Accepted April 2, 2026

DOI: 10.3892/etm.2026.13185

**Abstract.** 3D-printed prosthesis replacement is increasingly applied for reconstruction following resection of malignant bone tumors. However, the management of postoperative tumor recurrence with periprosthetic infection following surgery remains challenging, as clinical manifestations and imaging features can be obscured by or mimic tumor recurrence, periprosthetic biofilms render conventional antibiotics ineffective and large segmental bone defects limit reconstructive options. The present study reports the case of a 53-year-old female patient with cervical cancer who developed femoral metastasis and tumor recurrence with periprosthetic infection. A customized anatomically matched femoral prosthesis was designed using 3D printing technology. The patient underwent tumor resection, debridement and implantation of the custom prosthesis, followed by prolonged antibiotic therapy. The infection was effectively controlled and limb salvage was achieved. At 1 year postoperative follow-up, the patient was able to ambulate without assistance and reported no notable pain. Personalized 3D-printed prosthesis combined with appropriate antibiotic therapy may offer an effective treatment option for recurrent bone tumors complicated by infection and large segmental bone defects.

## Introduction

Cervical cancer is the fourth most common cancer in women globally, with ~660,000 new cases and ~350,000 associated deaths in 2022. Following the lung and liver, bone is the third-most common site of distant metastasis (1). The incidence of clinical bone metastasis in cervical cancer is 0.8-23.0% (2). Bone metastasis most frequently occurs in the axial skeleton, with the lumbar spine being the most common (36.4%), followed by the thoracic spine and the pelvis, while metastases to the femur, humerus and fibula are relatively rare (3). Unlike patients with early-stage or locally advanced cervical cancer who can be effectively treated with conventional therapies such as surgery, chemotherapy or radiotherapy, there is currently no standard treatment for patients with metastatic cervical cancer due to its heterogeneous manifestation (2). For bone metastasis, surgery should be considered. However, since most patients with bone metastasis die within 1 year, treatment should not only aim to improve quality of life and relieve pain but also prolong survival (4).

In recent years, the application of 3D-printed prostheses in orthopedic oncology has become increasingly widespread (5,6). These prostheses provide patient-specific implants that precisely match the morphology of bone defects, promote osseointegration through porous trabecular structures and improve surgical accuracy in complex limb-salvage procedures (6,7). These advantages are particularly valuable in cases involving extensive bone defect, tumor recurrence and periprosthetic infection, where conventional implants typically fail to meet the demands of such complex cases (5,6).

The present study reports a rare case of recurrent cervical cancer with femoral metastasis complicated by periprosthetic infection.

## Case report

*Patient history and preoperative preparation.* A 53-year-old female patient underwent a total hysterectomy due to cervical cancer 4 years before at an external hospital. In June 2024, the patient presented to the Department of Orthopaedics, Yunnan Cancer Hospital, The Third Affiliated Hospital of Kunming Medical University (Kunming, China) with pain in the left thigh

---

*Correspondence to:* Dr Yanbin Xiao, Department of Orthopaedics, Yunnan Cancer Hospital, The Third Affiliated Hospital of Kunming Medical University, 519 Kunzhou Road, Xishan, Kunming, Yunnan 650118, P.R. China  
E-mail: xiaoyanbin73@126.co

Dr Haixia Li, Department of Neurology, The First People's Hospital of Yunnan Province, 157 Jinbi Road, Xishan, Kunming, Yunnan 650118, P.R. China  
E-mail: haixiali6677@163.com

**Key words:** 3D printing, femur metastasis, tumor recurrence, infection

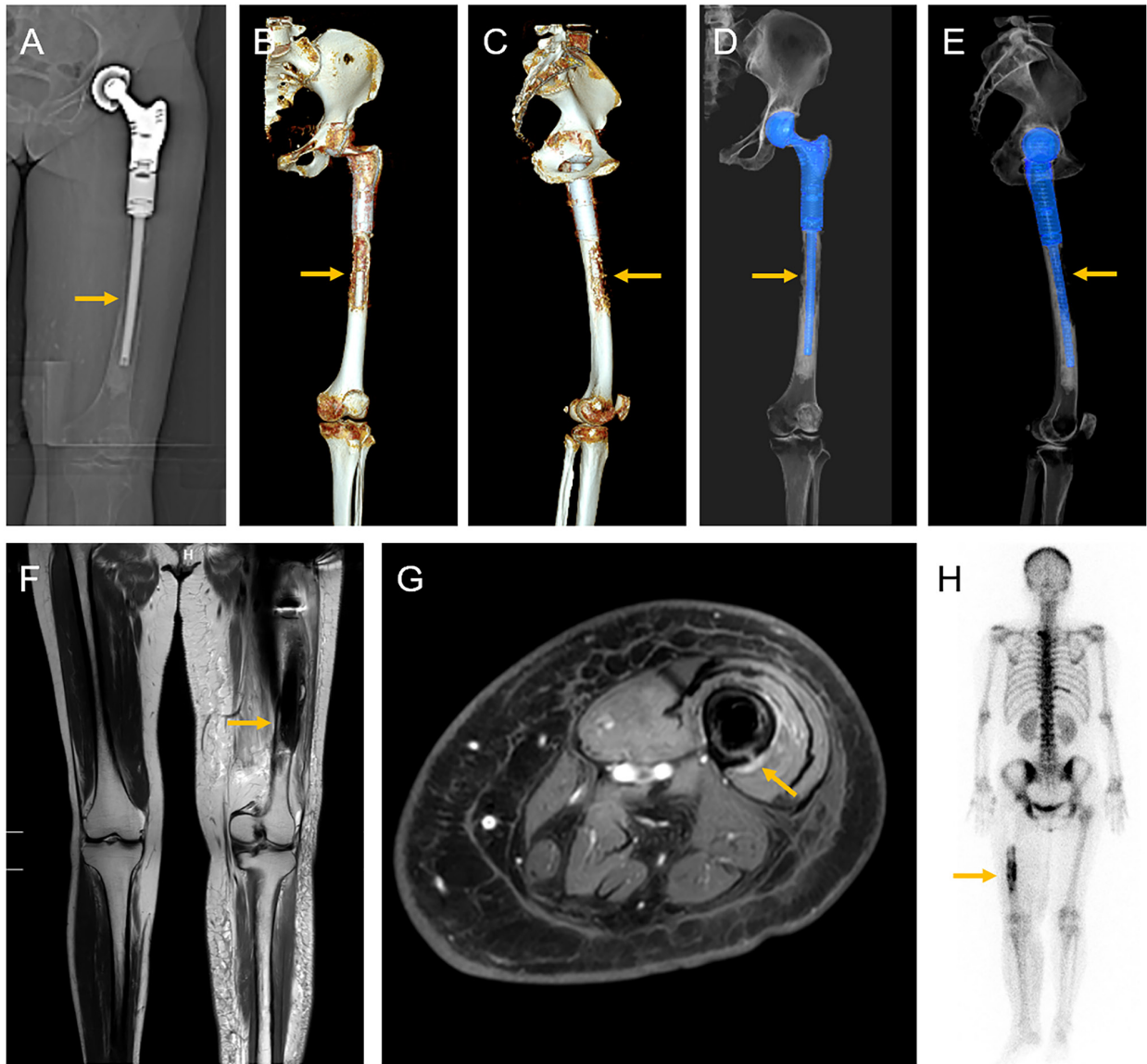


Figure 1. Preoperative imaging findings (June 2024). (A) X-ray showed osteolytic destruction of the distal femur around the primary prosthesis. (B) Coronal 3D CT reconstruction demonstrating distal femoral bone destruction (arrow). (C) Sagittal 3D CT reconstruction confirming prosthetic loosening and periprosthetic bone resorption (arrow). (D) Coronal 3D CT with segmented blue-colored prosthesis visualizing prosthetic loosening (arrow). (E) Sagittal 3D CT with segmented blue-colored prosthesis demonstrating prosthetic migration (arrow). (F) Sagittal MRI showing abnormal signal intensity in the distal femur and periprosthetic soft tissue (arrow). (G) Axial MRI revealing periprosthetic fluid collection and soft tissue edema (arrow). (H) Single photon emission computed tomography bone scan revealing abnormal radionuclide uptake in the left femoral stump (arrows), as well as in T2, T5 and T7 vertebrae.

and limited mobility. A total of 2 years later, tumor recurrence with metastasis to the left femur led to left hip arthroplasty. The patient was admitted in June 2024, with pain in the left thigh and limited mobility. Imaging examination (plain radiography: 60 kV, 10 mAsec; contrast-enhanced MRI: 3.0 T, Siemens Magnetom Skyra, slice thickness 4 mm) revealed bone destruction in the distal left femur, suggesting tumor recurrence, and the swelling of the left thigh was considered to be due to lymphatic atresia resulting from postoperative radiotherapy for cervical cancer (Fig. 1). Whole-body single photon emission computed tomography bone scans revealed multiple areas of abnormal increased bone metabolism throughout the skeletal system, including a solitary lesion in the left femur. Preoperative serum tumor markers, namely, cancer antigen (CA)72-4 (13.30 U/ml; normal range, <6.9 U/ml), carcino-embryonic antigen (804.0 ng/ml; normal range, <5.0 ng/ml

for smokers, <2.5 ng/ml for non-smokers), neuron-specific enolase (22.20 ng/ml; normal range, <16.3 ng/ml), squamous cell carcinoma antigen (2.20  $\mu\text{g/l}$ ; normal range, <1.5  $\mu\text{g/l}$ ), cancer CA-125 (35.3 U/ml; normal range, <35 U/ml) and CA19-9 (44.9 U/ml; normal range, <37 U/ml), were elevated. Preoperative hematological examination on the first day of admission showed: White blood cell count (WBC),  $4.89 \times 10^9/\text{l}$  (normal range,  $4.0\text{--}10.0 \times 10^9/\text{l}$ ); C-reactive protein, 5.31 mg/l (normal range, <5.0 mg/l); and erythrocyte sedimentation rate, 88 mm/h (normal range, 0–20 mm/h for women). Postoperative body temperature was normal, with no other sign of preoperative infection. Considering the patient history of cervical cancer, absence of other recorded tumor-related medical history and imaging findings demonstrating typical features of bone destruction, the preliminary diagnosis was metastatic cervical cancer to the left distal femur.

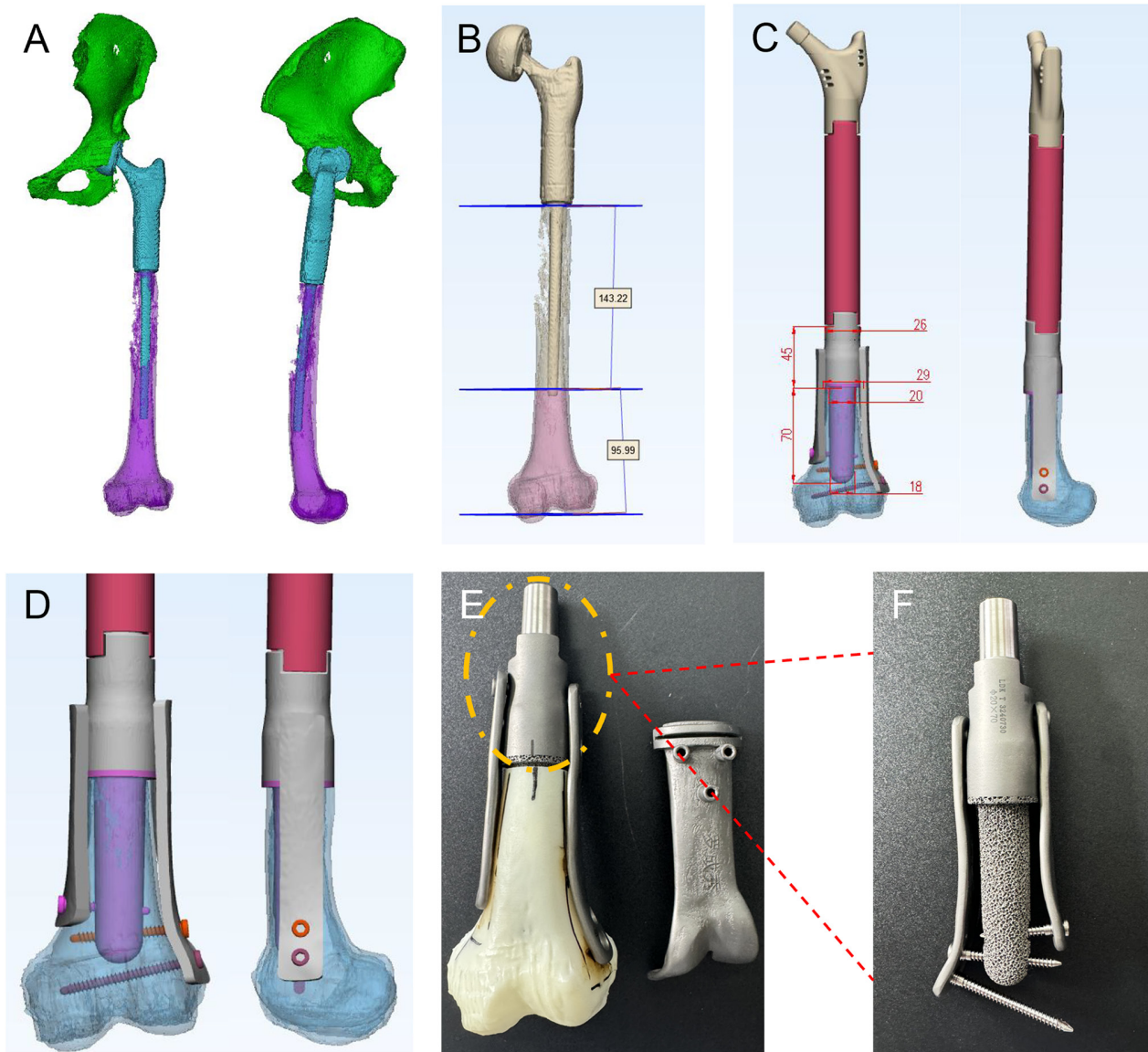


Figure 2. Design and fabrication of the 3D-printed customized femoral prosthesis. (A) 3D bone model reconstructed from CT data. (B) Surgical planning: The distal femur osteotomy was performed at 96 mm above the lateral condyle, with a total osteotomy length of 143 mm. (C) Complete assembly design of the modular prosthesis and 3D-printed implant with marked dimensional parameters. (D) 3D design of the distal femoral 3D-printed prosthesis, showing the integrated structure matching the residual femur. (E) Assembly diagram of the 3D-printed distal femoral prosthesis and residual femur mold, demonstrating the implant-bone fitting relationship. (F) The prosthesis-bone interface adopts a porous trabecular structure to promote osseointegration, with bilateral plates for distal fixation.

Due to notable bone destruction at the left distal femur, the surgeon opted for surgical resection of the distal femur lesion and performed reconstruction using a 3D-printed custom prosthesis (Fig. 2). Because the length of the distal medullary canal was short and intramedullary nail fixation could not provide sufficient stability, additional plates were applied on both sides of the construct to augment fixation. The interface between the prosthesis and the distal femur was composed of trabecular bone structure, which facilitated osseointegration and effectively decreased the risk of mechanical complications, such as long-term loosening and fracture. The 3D printed artificial femur prosthesis was designed and manufactured by Beijing Lidakang Technology Co., Ltd.

*Surgical procedure and postoperative diagnosis.* A 30 cm surgical incision was made along the lateral left thigh to

expose the proximal femoral shaft prosthesis. Fluid accumulation was observed around the prosthesis, and a sample was collected for microbiological analysis. The upper femoral segment wound was protected with sterile gauze, while the lower femoral segment was exposed. The bone destruction in the middle of the left femur was notable, accompanied by a soft tissue mass. A femoral osteotomy was performed 9.6 cm above the lateral femoral condyle of the distal femur. After complete incision of the scarred hip capsule, the hip prosthesis and distal femur were removed. When the hip prosthesis was separated from the distal femur, yellow-white pus was observed around the prosthesis, and the pus was retained to detect microorganisms. The tissue around the hip prosthesis and the middle and upper femur, including scar and necrotic tissue, was completely removed. The wound was rinsed with iodophor and hydrogen peroxide five times, and surgical gloves

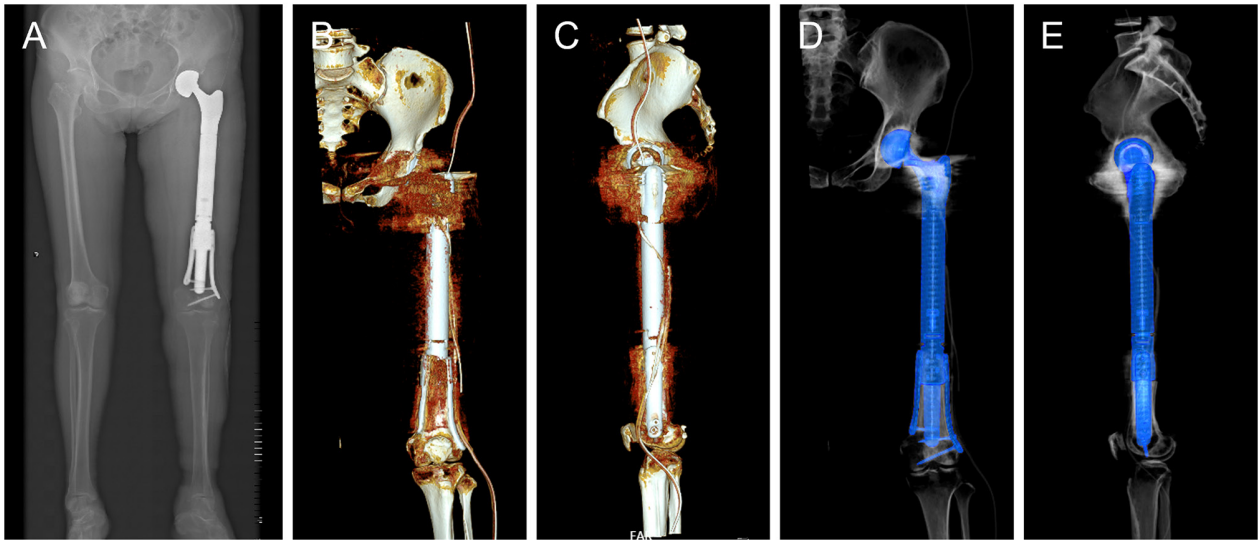


Figure 3. Postoperative imaging at day 3. (A) X-rays showed satisfactory positioning of the 3D-printed distal femoral prosthesis and modular tumor-type hemi-hip prosthesis. (B) Coronal 3D CT reconstruction shows stable fixation of the prosthesis to the residual femur. (C) Sagittal 3D CT reconstruction confirms excellent apposition and stable fixation between the implant and residual femur. (D) Coronal 3D CT with segmented blue-colored prosthesis visualizes satisfactory prosthesis position and stability. (E) Sagittal 3D CT with segmented blue-colored prosthesis visualizes secure fixation of the implant.

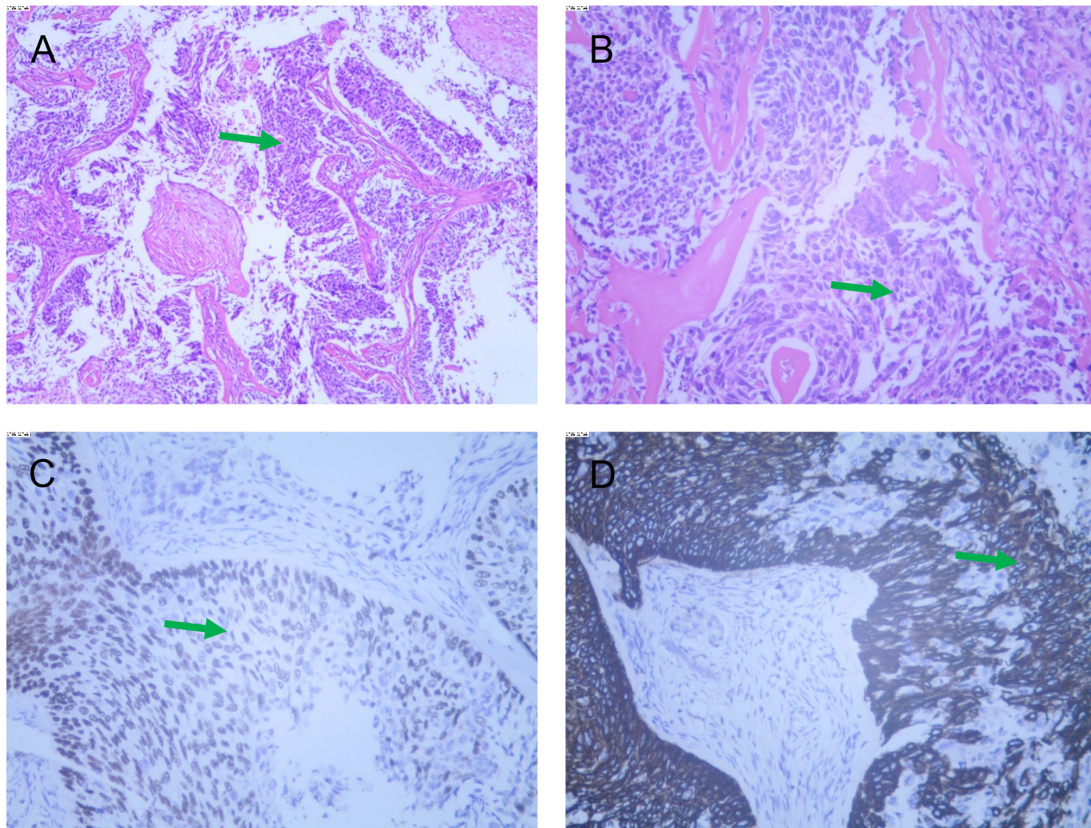


Figure 4. Histopathological and immunohistochemical findings. (A) Hematoxylin and eosin (H&E) staining (original magnification, x40) shows heterotypic tumor cell nests within fibrous stroma, consistent with metastatic poorly differentiated carcinoma (arrow). (B) Hematoxylin and eosin (H&E) staining (original magnification, x100) demonstrates malignant heterotypic cells in fibrous tissue, confirming metastatic poorly differentiated carcinoma (arrow). (C) Immunohistochemical staining (original magnification, x40) shows positive expression of squamous differentiation markers in tumor cells, supporting squamous differentiation (arrow). (D) Immunohistochemical staining (original magnification, x100) confirms strong positive expression of squamous differentiation markers in tumor cell nests (arrow).

and sheets were replaced. The 3D-printed distal femoral prosthesis was implanted into the medullary cavity of the femur retention segment and the upper segment of the prosthesis was

connected to the newly implanted modular tumor type half-hip prosthesis. The wound was irrigated twice with iodophor saline and hydrogen peroxide. Following surgery, the left lower

Table I. Antimicrobial susceptibility.

Antibiotic	MIC, mg/l	Interpretation	Reference range, mg/l
Ciprofloxacin	≤0.50	S	1.00-4.00
Clindamycin	≤0.25	S	0.50-4.00
Erythromycin	≤0.25	S	0.50-8.00
Gentamicin	≤0.50	S	4.00-16.00
Linezolid	2.00	S	4.00-8.00
Levofloxacin	≤0.12	S	1.00-4.00
Moxifloxacin	≤0.25	S	0.50-2.00
Furantoin	≤16.00	S	32.00-128.00
Oxacillin	0.50	S	2.00-4.00
Penicillin	≥0.50	R	0.13-0.25
Rifampicin	≤0.50	S	1.00-4.00
Cotrimoxazole	≤0.50	S	2.00-4.00
Tetracycline	2.00	S	4.00-16.00
Tigacycline	≤0.12	S	≤0.50
Vancomycin	≤0.50	S	4.00-32.00

MIC, minimum inhibitory concentration; S, susceptible; R, resistant.

limb was placed in a T-shape shoe to prevent external rotation and maintained in 30° of abduction with neutral rotation. A total of 3 days after the surgery, the lumbar spine anteroposterior and lateral X-ray and CT scan showed that 3D printed artificial femoral prosthesis and modular tumor type half-hip prosthesis. were in good position and the intervertebral height was satisfactory (Fig. 3).

Routine hematoxylin and eosin (HE) staining (10% neutral buffered formalin, room temperature, 24 h; 4-μm sections; hematoxylin 5 min, eosin 1 min, at room temperature; light microscope) was performed on the pathological specimens and re-evaluation of the immunological marker. Heterotypic cell nest specimens were found between the fibrous tissue and no clear malignant tumors were found at the four incisal margins of soft tissue and the pulp cavity of the broken end. Immunohistochemical (IHC) staining was performed on formalin-fixed, paraffin-embedded tissue sections as previously described (8), and the IHC results were as follows: Pan cytokeratin (CK)(+), vimentin(-), CK7(+), CK20(-), synaptophysin(-), chromogranin A(-), CD56(-), Ki-67(+, ~60%), tumor protein p63 (p63)(partially +), p40(partially +), CK5/6(partially +), CD10(-), high molecular weight CK(partially +), thyroid transcription factor-1(-), napsin A(-) and thyroglobulin(-) (Fig. 4). HE staining and immunohistochemical results supported the diagnosis of metastatic poorly differentiated carcinoma, with a phenotype indicating squamous differentiation. Cervical cancer metastasis was first considered in combination with medical history. Pus was observed around the prosthesis and the bacterial culture was positive for *Staphylococcus lugdunensis*. Combined with pathological and microbial culture results, the postoperative diagnosis was recurrence of cervical cancer with metastasis to the left femur accompanied by periprosthetic infection of the left femoral prosthesis.

*Postoperative treatment and follow-up.* According to the results of microbial culture and drug sensitivity test (Table I), intravenous cefazolin sodium (1 g) was administered three times daily combined with oral rifampicin 300 mg twice daily during the 1 month antibiotic treatment period. Postoperative infection markers (C-reactive protein, ESR, procalcitonin) were monitored daily; these markers rose on postoperative days 2-3, followed by a gradual decline and return to normal by postoperative day 90 (Fig. 5). In addition, the patient body temperature remained normal following surgery. Bacterial culture was performed on wound drainage every 2 days and the results were negative for bacterial growth. The patient underwent outpatient follow-up visits at 1, 2 and 12 months postoperatively, with no postoperative complications observed during this period. X-ray and CT scan at 12 months after surgery demonstrated satisfactory positioning of the prosthesis without any signs of loosening, periprosthetic infection and fracture. In addition, no bone absorption was observed between the distal residual femur and the prosthesis and new bone growth was evident within the trabecular structure of the 3D-printed prosthesis. The patient was asymptomatic at the 12-month follow-up in June 2025, walking without a crutch and reported a visual analog scale score (9) of 0 for left thigh pain (Fig. 6).

## Discussion

Cervical cancer is a notable burden in developing countries. Bone is the third most common site of distant metastasis after the lung and liver (3). Among patients with bone recurrence, 62-93% experience bone-related symptoms, such as bone pain or neurological deficit (3,10). Diagnostic imaging techniques such as bone scan, CT, MRI and 18F-fluorodeoxyglucose (<sup>18</sup>FDG)-positron emission tomography are widely used for the diagnosis of bone metastasis. In the present patient, a bone scan performed 2 years after cervical cancer surgery demonstrated abnormal nuclide concentration in the left proximal femur, suggesting recurrence of cervical cancer with bone metastasis. Subsequently, left hip prosthesis replacement was performed and the postoperative pathology confirmed bone metastasis. Therefore, scanning served an important role in detecting bone metastasis. Treatment strategies for patients with cervical cancer accompanied by bone metastasis are complex and require consideration of factors such as the primary treatment, metastasis site, recurrence-free interval, metastasis symptoms and ECOG performance status (11) when determining whether to employ surgery, chemotherapy and/or radiotherapy (12). Patients with bone metastasis typically have a poor prognosis, with a 5-year overall survival rate of ~10% after bone recurrence (13).

Tumor-type endoprostheses have facilitated limb-salvage procedures in primary bone and soft tissue sarcomas and are increasingly being used in symptomatic metastases of the long bones (14,15). Although artificial joint implantation improves patient quality of life, it is often accompanied by complications, including aseptic failure and prosthetic joint infection (PJI). The diagnosis and optimal treatment of PJI remains a challenge. Early postoperative and acute hematogenous infection are typically easier to identify, but late-onset chronic infection is difficult to predict. Clinical signs and symptoms,

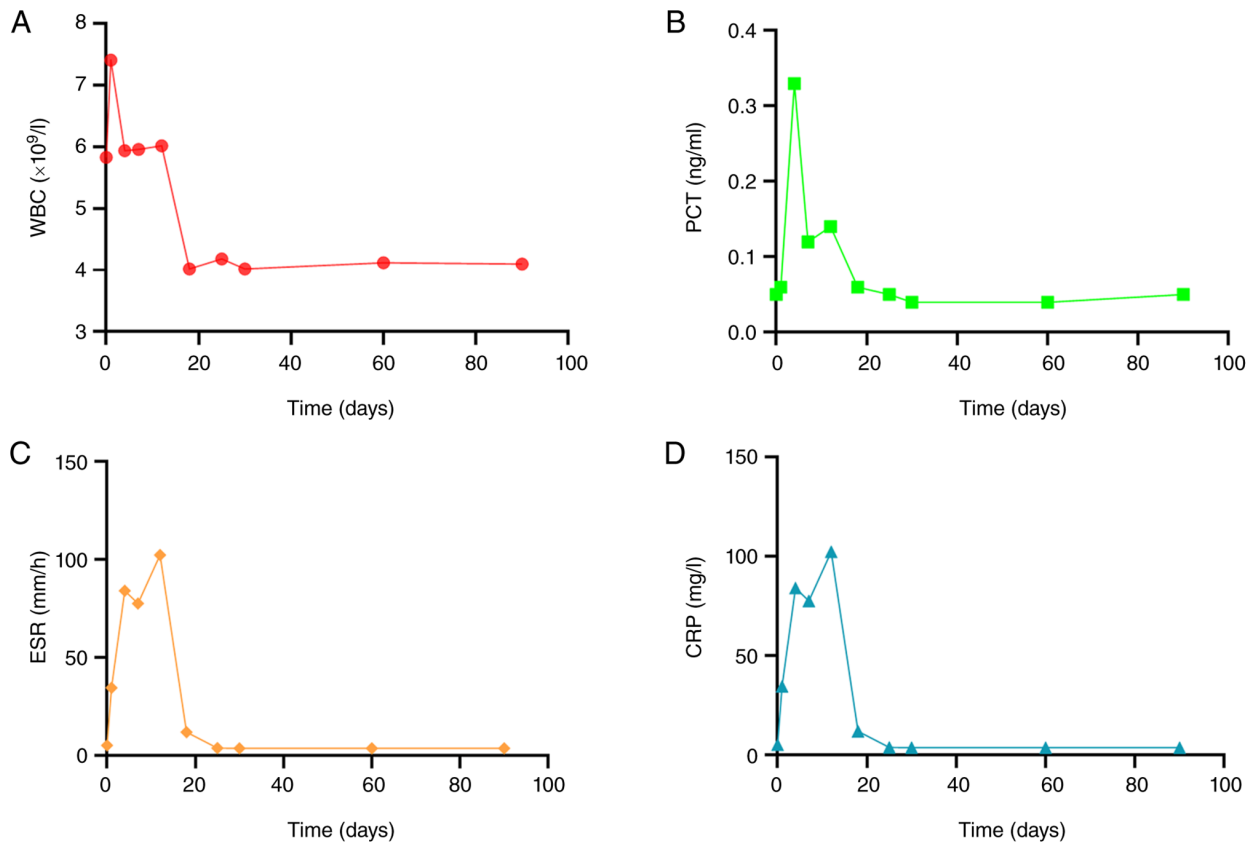


Figure 5. Perioperative changes in infection indicators. (A) WBC, (B) PCT, (C) ESR and (D) CRP peaked on postoperative days 2-3 and gradually returned to normal levels within 1 month after surgery. WBC, white blood cell; PCT, procalcitonin; CRP, C-reactive protein; ESR, erythrocyte sedimentation rate.

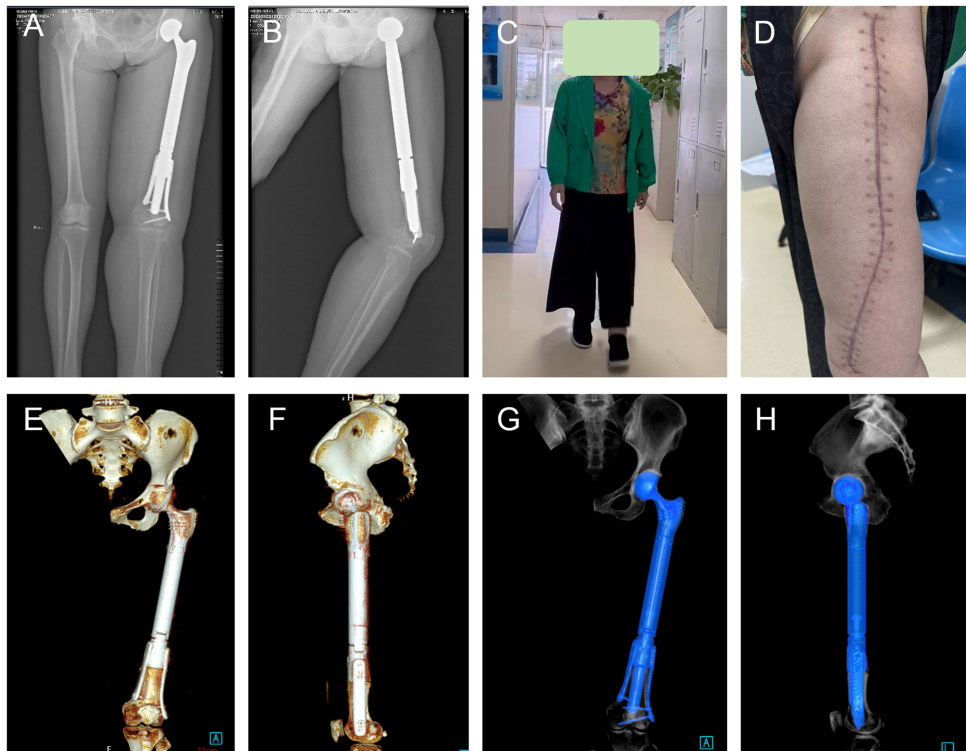


Figure 6. Postoperative imaging and functional outcome after 1 year. (A) Coronal X-ray showing stable prosthesis position without loosening or fracture. (B) Sagittal X-ray demonstrating satisfactory prosthesis alignment and fixation. (C) Clinical photograph of the patient walking independently without assistive devices. (D) Clinical photograph showing well-healed surgical wound at the operative site. (E) Coronal 3D CT reconstruction revealing good prosthesis-residual femur interface fitting, no bone resorption or prosthesis loosening. (F) Sagittal 3D CT reconstruction confirming satisfactory prosthesis position, secure fixation and close contact with the residual femur. (G) Coronal 3D CT with segmented blue-colored prosthesis visualizes satisfactory prosthesis position and stability. (H) Sagittal 3D CT with segmented blue-colored prosthesis visualizes secure fixation of the implant.

laboratory tests, radiography and joint aspiration are insensitive and non-specific (16). In addition, artifacts produced by the prosthetic devices interfere with tomographic imaging techniques such as CT and MRI. In the present patient, imaging studies showed no evidence of periprosthetic infection and the levels of CRP, procalcitonin and WBC, which are indicators of infection, were in normal range, although ESR was elevated. Additionally, patients with malignant tumors or periprosthetic infection may also have elevated ESR (17). Bone scans suggested recurrence of periprosthetic bone metastases. Considering the patient history of cervical cancer bone metastasis, there was concern about the recurrence of bone metastasis around the femoral prosthesis. Periprosthetic infection can be easily overlooked, as its clinical manifestations and imaging features may be obscured by or mimic tumor recurrence. In the present case, preoperative bone scintigraphy suggested tumor recurrence but failed to detect periprosthetic infection, which was only confirmed intraoperatively. This highlights the limitation of bone scans in distinguishing infection from tumor-associated inflammation. 18F-FDG PET-CT may offer an enhanced imaging modality for more accurate characterization of lesions by integrating anatomical and metabolic imaging (18). As demonstrated by Mulita *et al* (19), PET-CT scan detects occult lesions and improve target delineation in 76.5% of patients. PET-CT exhibits higher sensitivity in characterizing metabolically active lesions, which may improve preoperative diagnostic accuracy in complex cases, guiding surgical planning and potentially avoiding unexpected intraoperative findings (20). Beyond precise diagnosis, Internet of Surgical Things (IoST) enables early detection of complications and improves surgical precision to optimize patient management. As highlighted by Mulita *et al* (21), the IoST enhances healthcare through remote surgery and continuous patient monitoring. In the context of bone tumor recurrence and infection, perioperative remote monitoring could enable early detection of recurrent infection or mechanical complications, while IoST-based systems integrate preoperative 3D planning with intraoperative navigation, thereby improving surgical precision. Thus, incorporating IoST technology into multidisciplinary bone tumor management may facilitate more responsive healthcare delivery.

3D printing, also known as additive manufacturing, converts digital models into physical objects through a process beginning with computer-aided design and converting images into standard triangular mesh files readable by printers. Since its emergence in the 1980s, its applications in medicine have expanded rapidly. An early report described the use of stereolithography to create cardiac structural models, which were used to optimize surgical planning (6). In bone tumors, 3D printing technology enables the fabrication of customized prostheses that precisely match the morphology of bone defects, facilitates preoperative simulation to enhance surgical accuracy and allows design of porous trabecular structures at the bone-implant interface to promote osseointegration (22). These capabilities are valuable in complex cases involving large bone defect, tumor recurrence and periprosthetic infection, where conventional implants typically fail to meet clinical requirements (23). Lu *et al* (6) performed segmental resection of malignant bone tumors in the bone shaft with 3D printed titanium alloy

prosthesis replacement and reported all cases achieved limb function recovery and prosthesis stability. The present study reconstructed a large segmental bone defect after tumor resection using a 3D-printed femoral prosthesis, resulting in a favorable clinical outcome. The present case reports the concurrent management of tumor recurrence and periprosthetic infection, which are challenging complications rarely reported together. The primary mechanism underlying periprosthetic infection involves pathogenic bacteria colonizing the surface of joints and forming irreversible biofilms. The biofilms formed by pathogens around the prosthesis render conventional antibiotics ineffective (24). Studies have confirmed that only rifampicin and quinolones effectively eradicate bacteria in biofilms (25,26). Therefore, rifampicin was administered to the present patient for 1 month after surgery and the infection was well controlled without recurrence.

In conclusion, 3D-printed prostheses provide a promising reconstructive option for large extensive bone defect following tumor resection. Combined surgical debridement and with targeted antibiotic therapy may effectively control periprosthetic infection and enable successful limb salvage.

#### Acknowledgements

Not applicable.

#### Funding

The present study was supported by the National Natural Science Foundation of China (grant no. 82301534), the Basic Research Project of Yunnan Province (grant no. 202401CF070010), the High-Level Talent Introduction Program of Yunnan Provincial Health Commission (grant no. 2023-KHRCBZ-B17), the First-level Discipline Team of Kunming Medical University (grant no. 2024XKTDYS05), the Scientific Research Fund Project of Yunnan Provincial Department of Education (grant no. 2024J0244) and the Science and Technology Plan Project of Yunnan Provincial Department of Science and Technology (grant no. 202501CF070030).

#### Availability of data and materials

The data generated in the present study are included in the figures and/or tables of this article.

#### Authors' contributions

JL wrote the manuscript. JL and HL revised the manuscript. YZ, JK, YN and SC performed follow-up. CT collected associated references. JL and CT performed the analysis and interpretation of data. YX and HL conceived the study and edited the manuscript. All authors have read and approved the final manuscript. JL and YX confirm the authenticity of all the raw data.

#### Ethics approval and consent to participate

Not applicable.

## Patient consent for publication

Informed consent was obtained from the patient for the publication of this case report, including the publication of all images, clinical data and other data included in the manuscript.

## Competing interests

The authors declare that they have no competing interests.

## References

- Gioe A, Arciuolo D, Carbone V, Zannoni G, Gambacorta MA, Maccauro G, Scambia G and Corrado G: Isolated humeral metastasis in cervical cancer: A case report and review of the literature. *J Cancer Res Ther* 18: 273-276, 2022.
- Li H, Wu X and Cheng X: Advances in diagnosis and treatment of metastatic cervical cancer. *J Gynecol Oncol* 27: e43, 2016.
- Thanappapasr D, Nartthanarung A, Likittanasombut P, Na Ayudhya NI, Charakorn C, Udomsubpayakul U, Subhadarbandhu T and Wilailak S: Bone metastasis in cervical cancer patients over a 10-year period. *Int J Gynecol Cancer* 20: 373-378, 2010.
- van Meir H, Kenter GG, Burggraaf J, Kroep JR, Welters MJ, Melief CJ, van der Burg SH and van Poelgeest MI: The need for improvement of the treatment of advanced and metastatic cervical cancer, the rationale for combined chemo-immunotherapy. *Anticancer Agents Med Chem* 14: 190-203, 2014.
- Huang X, Huang D, Lin N, Yan X, Qu H and Ye Z: 3D-Printed prosthesis with an articular interface for anatomical acetabular reconstruction After Type I + II (+ III) Internal Hemipelvectomy: Clinical outcomes and finite element analysis. *J Bone Joint Surg Am* 107: 184-195, 2025.
- Anagnostopoulos S, Baltayiannis N, Koletsis NE, Mulita F, Spanou F, Leivaditis V, Katsakiori P, Tsakalidis G, Nikolakopoulos K and Mitsos S: 3D printing in medicine: Bridging imaging, education, and practice. *Arch Med Sci Atheroscler Dis* 10: e172-e188, 2025.
- Lu Y, Chen G, Long Z, Li M, Ji C, Wang F, Li H, Lu J, Wang Z and Li J: Novel 3D-printed prosthetic composite for reconstruction of massive bone defects in lower extremities after malignant tumor resection. *J Bone Oncol* 16: 100220, 2019.
- Magaki S, Hojat SA, Wei B, So A and Yong WH: An introduction to the performance of immunohistochemistry. *Methods Mol Biol* 1897: 289-298, 2019.
- Huskisson EC: Measurement of pain. *Lancet* 2: 1127-1131, 1974.
- Nartthanarung A, Thanappapasr K, Udomsubpayakul U and Thanappapasr D: Age and survival of cervical cancer patients with bone metastasis. *Asian Pac J Cancer Prev* 15: 8401-8404, 2014.
- Oken MM, Creech RH, Tormey DC, Horton J, Davis TE, McFadden ET and Carbone PP: Toxicity and response criteria of the Eastern Cooperative Oncology Group. *Am J Clin Oncol* 5: 649-655, 1982.
- Atjimakul T and Hanprasertpong J: Clinical outcomes and their prognostic factors among cervical cancer patients with bone recurrence. *Obstet Gynecol Int* 2022: 3446293, 2022.
- Kim TH, Kim MH, Kim BJ, Park SI, Ryu SY and Cho CK: Prognostic importance of the site of recurrence in patients with metastatic recurrent cervical cancer. *Int J Radiat Oncol Biol Phys* 98: 1124-1131, 2017.
- Smolle MA, Andreou D, Tunn PU and Leithner A: Advances in tumour endoprostheses: A systematic review. *EFORT Open Rev* 4: 445-459, 2019.
- Kendal JK, Hamad CD, Abbott AG, Greig D, Trikha R, Christ AB, Wessel LE, Puloski SKT, Monument MJ and Bernthal NM: What are the indications and survivorship of tumor endoprosthetic reconstructions for patients with extremity metastatic bone disease? *J Surg Oncol* 127: 1196-1202, 2023.
- Cobo J and Del Pozo JL: Prosthetic joint infection: Diagnosis and management. *Expert Rev Anti Infect Ther* 9: 787-802, 2011.
- Brigden ML: Clinical utility of the erythrocyte sedimentation rate. *Am Fam Physician* 60: 1443-1450, 1999.
- Mulita A, Bekou E, Valsamaki P, Koukourakis IM, Mulita F, Liolis E, Zissimopoulos A, Giatromanolaki A and Koukourakis MI: 18F-FDG PET-CT-vs. CT-Based radiotherapy treatment planning for head and neck cancer. *Life (Basel)* 16: 263, 2026.
- Mulita A, Valsamaki P, Bekou E, Anevlavis S, Nanos C, Zissimopoulos A, Giatromanolaki A and Koukourakis MI: Benefits from 18F-FDG PET-CT-based radiotherapy planning in stage III Non-small-cell lung cancer: A prospective Single-center study. *Cancers (Basel)* 17: 1969, 2025.
- Li L, Hu X, Ma J, Yang S, Gong W and Zhang C: A systematic review of [68Ga]Ga-DOTA-FAPI-04 and [18F]FDG PET/CT in the diagnostic value of malignant tumor bone metastasis. *Front Oncol* 12: 978506, 2022.
- Mulita F, Verras GI, Anagnostopoulos CN and Kotis K: A smarter health through the internet of surgical things. *Sensors (Basel)* 22: 4577, 2022.
- Park JW and Kang HG: Application of 3-dimensional printing implants for bone tumors. *Clin Exp Pediatr* 65: 476-482, 2022.
- Liang H, Guo W, Yang Y, Li D, Yang R, Tang X and Yan T: Efficacy and safety of a 3D-printed arthrodesis prosthesis for reconstruction after resection of the proximal humerus: Preliminary outcomes with a minimum 2-year follow-up. *BMC Musculoskelet Disord* 23: 635, 2022.
- Almasri D and Dahman Y: Prosthetic joint infections: Biofilm formation, management, and the potential of mesoporous bioactive glass as a new treatment option. *Pharmaceutics* 15: 1401, 2023.
- Zimmerli W: Clinical presentation and treatment of orthopaedic implant-associated infection. *J Intern Med* 276: 111-119, 2014.
- Aboltins C, Daffy J, Choong P and Stanley P: Current concepts in the management of prosthetic joint infection. *Intern Med J* 44: 834-840, 2014.



Copyright © 2026 Li et al. This work is licensed under a Creative Commons Attribution-NonCommercial-NoDerivatives 4.0 International (CC BY-NC-ND 4.0) License.